NJC

PAPER

View Article Online
View Journal | View Issue

Cite this: *New J. Chem.*, 2022, **46**, 16309

Hydrolytic dehydrogenation of ammonia borane in neat water using recyclable zeolite-supported cyclic alkyl amino carbene (CAAC)–Ru catalysts†

Áron Balla,[a] Márton Nagyházi,[a] Gábor Turczel,[a] Hanna E. Solt,[a] Magdolna R. Mihályi,[a] Jenő Hancsók,[b] József Valyon,[a] Tibor Nagy,[c] Sándor Kéki,[c] Paul T. Anastas[d] and Róbert Tuba *[a]

Cyclic alkyl amino mono- and bis-carbene ruthenium (CAAC–Ru) complexes were immobilized on mesoporous Y zeolite (catalysts **3** and **4**) and showed high activity and stability in ammonia borane (**AB**) hydrolytic dehydrogenation. Both catalysts have a Ru content as low as 0.1 wt%. Catalysts **3** and **4** provide a reasonable activity even at a loading of 10 ppm (0.001 mol%) giving a turnover number (TON) of 79 000 mol_{H_2} mol_{cat}^{-1}. The optimal loading, however, was found to be slightly higher for catalyst **4**, at around 50 ppm (0.005 mol%), giving a turnover frequency (TOF) of 8500 mol_{H_2} mol_{cat}^{-1} h^{-1} and a TON of 49 375 mol_{H_2} mol_{cat}^{-1} whilst retaining a high nH_2/n**AB** ratio (2.51). This value is higher than those observed for its homogeneous analogue **2** (TOF, 7500 mol_{H_2} mol_{cat}^{-1} h^{-1}; TON, 43 600 mol_{H_2} mol_{cat}^{-1}; released nH_2/n**AB** ratio, 2.18). Interestingly, it was found that the zeolite-supported catalyst gave a better performance than the non-supported water-soluble derivatives. No ruthenium leaching was detected for any of the zeolite-supported systems. Catalyst **4** showed a significantly higher activity than catalyst **3** and could be recycled up to 10 times. Catalyst **4** demonstrated a reasonable hydrolytic dehydrogenation activity even after three days in water upon exposure to air. The highest TON (79 000 mol_{H_2} mol_{cat}^{-1}) obtained with catalyst **4** is equal to 1.68 kg H_2 per gram of ruthenium metal.

Received 6th July 2022,
Accepted 25th July 2022

DOI: 10.1039/d2nj03334h

rsc.li/njc

Introduction

Nowadays one of the biggest challenges for the energy industry is the transition from fossil-fuel power sources to renewable ones.[1] Therefore, the need for the higher exploitation of renewable energy is now clear in all segments of the energy industry. The biggest criticism of using such resources is the problem of availability, as most renewable power is not accessible during the hours of the highest demand.[2] This mismatch in power distribution can be overcome by introducing the electrolysis of water as a power-conversion method, which converts electricity into storable hydrogen.[3] Hydrogen has the highest energy content of any chemical fuel, which makes it cost effective; moreover, it is environmentally friendly.[4] The hydrogen can be safely stored in hydrogen-containing chemicals, including ammonia borane (**AB**), metal hydrides, synthetic hydrocarbons, carbohydrates and polyols.[5–8] Among these materials, **AB** shows high potential due to its high hydrogen-storage capacity (19.6 wt%) and stability even in aqueous solution[9–11] compared with common metal hydrides, which are usually flammable and decompose readily upon contact with water.[12,13] **AB** is extremely light and involves only non-toxic, inexpensive elements (B, N, and H), which are available in large quantities.[14,15] The **AB** hydrolytic dehydrogenation is actually a two-step tandem reaction that involves the evolution of two moles of hydrogen from **AB** and one of hydrogen from water upon reaction with the *in situ*-formed borazine intermediate. Consequently, water takes part in the process not only as an environmentally benign reaction medium but also as a hydrogen fuel source.[16–20] Furthermore, the hydrolytic dehydrogenation of **AB** provides borates (B–O), which are entirely harmless to the environment. Borates can be converted to $NaBH_4$, an **AB** intermediate, *via* direct hydrogenation using molecular hydrogen and Mg (Scheme 1).[21]

[a] *Eötvös Loránd Research Network, Research Centre for Natural Sciences, Institute of Materials and Environmental Chemistry, Magyar tudósok körútja 2., 1519 Budapest, P.O. Box 286, Hungary. E-mail: tuba.robert@ttk.hu*
[b] *Research Centre for Biochemical, Environmental and Chemical Engineering, Department of MOL Hydrocarbon and Coal Processing, University of Pannonia, Egyetem u. 10, H-8210 Veszprém, Hungary*
[c] *Department of Applied Chemistry, Faculty of Science and Technology, University of Debrecen, Egyetem tér 1, H-4032 Debrecen, Hungary*
[d] *Yale Center for Green Chemistry and Engineering, Yale University, New Haven, Connecticut 06511, USA*

† Electronic supplementary information (ESI) available. See DOI: https://doi.org/10.1039/d2nj03334h

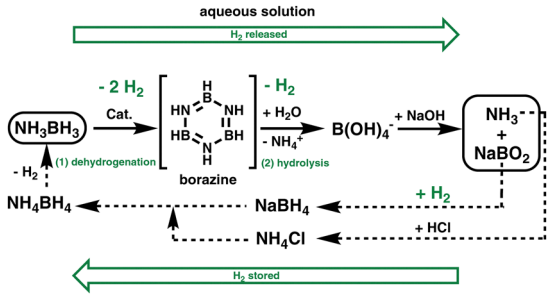

Scheme 1 Dehydrogenation and regeneration of ammonia borane under aqueous, hydrolytic conditions.

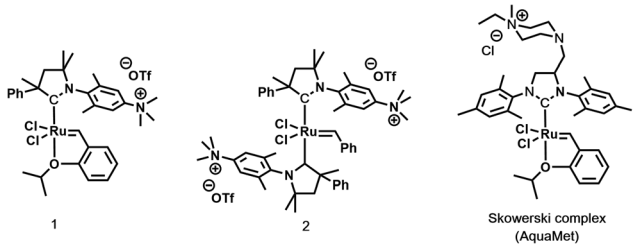

Fig. 1 Quaternary ammonium-ion-tagged Ru complexes with CAAC (**1** and **2**)[46] and NHC (the Skowerski-type complex, AquaMet).[47] (OTf^-, trifluoromethanesulfonate.)

In general, hydrogen can be liberated from **AB** either by heating (above 120 °C)[22] or catalytic hydrolytic dehydrogenation under ambient conditions.[23–26] From a sustainability and green chemistry point of view, the catalytic dehydrogenation reactions are the most preferable choices. A wide range of catalysts, including homogeneous and heterogeneous catalysts, have been demonstrated to induce the dehydrogenation of **AB**.[20,23,24,27–37] However, although more and more efficient catalyst systems have been reported, some drawbacks still remain. Nevertheless, some heterogeneous catalyst systems are considered to be ideal, which render relatively low turnover frequency (TOF) and turnover number (TON) values.[24] Moreover, the passivation of a metal surface by metaborate ions at a high **AB** concentration may deactivate the active centers. Consequently, their activity decreases steadily during the reaction, and thus long reaction times (up to 10 days) are often needed to achieve high TONs.[38] This can be overcome using highly active homogeneous catalysts. However, in most cases these catalysts are non-recyclable and require the use of common organic solvents. While being less environmentally benign,[39,40] the dehydropolymerization of **AB** in these solvents may occur to give stable, boron-containing inorganic polymers $((B–H)_n)$[16,30,41] that can be recycled to **AB**.[42]

As a new class of ligands used in homogeneous catalysis, cyclic alkyl amino carbenes (CAAC) appeared in the last decade.[43] Apparently, CAACs provide a better transition-complex stabilizing effect than phosphine and nitrogen heterocyclic carbene (NHC) ligands due to their better σ-donor and π-acceptor properties. The discovery of NHC[44] and CAAC[43] ligands enabled the synthesis of highly robust, moisture- and air-stable transition metal complexes. These complexes can be used in non-polar, organic media; however, going forward to sustainable catalysis, environmentally benign protic reaction media are preferred over volatile, flammable, and often toxic organic solvents. By modification of the ligands *via* the introduction of ionic (quaternary ammonium or sulfonate group)[45] tags, the complex becomes more hydrophilic, rendering reasonable water solubility. Following the same principles, our research group has recently reported the synthesis of ionic-tagged CAAC-ligand-containing Ru catalysts **1** and **2** (Fig. 1).[46]

Following this, we found that the quaternary ammonium-ion-tagged CAAC–Ru complexes show not only an exceptionally high olefin metathesis activity in protic media but also an outstanding **AB** hydrolytic dehydrogenation activity (TON = 86 100 mol_{H_2} mol_{cat}^{-1}, TOF up to 8620 mol_{H_2} mol_{cat}^{-1} h^{-1}) in neat water at a very low catalyst (**2**) loading of 10 ppm (Table 2). The evolved hydrogen can be as high as 2.91 nH$_2$/n**AB**.[31] The reaction yields non-hazardous borates in up to 99% yield, which are considered as a recyclable commodity material for hydrogen-storage systems (Scheme 1).[31]

The immobilization of organometallic complexes on a solid support has several advantages including catalyst recyclability. Amorphous and ordered mesoporous silica materials (such as MCM-41 and SBA-15) have been widely applied as supports for the immobilization of metal–NHC complexes.[48] In a general covalent grafting process, either the carbenes or the supports are first functionalized and then linked together *via* Si–O bonds. Zeolites with mesopores, such as hierarchical ZSM-5[49] and ITQ-2 type delaminated zeolite,[50] can also be used for the heterogenization of metal–carbene complexes. The catalytic activity of such supported complexes has been demonstrated in several reactions including olefin metathesis.[51,52]

Here, we apply a simple immobilization procedure, without a functionalization step using commercially available mesoporous zeolite Y. The quaternary ammonium-ion tags of the complexes can not only increase the activity of the catalyst in aqueous phase reactions but also bind the complex irreversibly to the negatively charged zeolite framework through electrostatic interactions. Zeolite-supported ionic Skowerski-type catalysts are well-known as highly active solid-supported olefin metathesis catalysts.[53–57] It is envisioned that the immobilized homogeneous catalyst systems **1** and **2** could provide suitable alternatives for environmentally benign, aqueous solution-based **AB** hydrogen-storage devices.

Results and discussion

Catalyst synthesis and characterization

Preliminary investigations revealed that single-quaternary-ammonium-ion-substituted complexes such as **1** and **2** can be readily impregnated in the H-zeolite support *via* simple H^+/–NMe_3^+ ion exchange.[53–55,57]

Zeolite Y has a three-dimensional pore structure characterized by large, spherical supercages with pore openings of 0.74 nm. It is known that the hydrothermal stability can be improved using controlled steaming and washing/leaching cycles to obtain an ultra-stable FCC catalyst to be used for catalytic cracking in

Table 1 Textural properties of the HY zeolite and zeolite-supported Ru complexes

Support/catalyst	SSA[a] ($m^2\ g^{-1}$)	V_{micro}[b] ($cm^3\ g^{-1}$)	V_{meso}[c] ($cm^3\ g^{-1}$)
HY (Si/Al = 15)	920	0.282	0.134
Catalyst **3**	734 (20%)	0.226 (20%)	0.105 (22%)
Catalyst **4**	747 (19%)	0.234 (18%)	0.102 (24%)

[a] Specific surface area (SSA) determined *via* the Brunauer–Emmett–Teller (BET) method. [b] V_{micro} calculated using the *t*-plot method. [c] $V_{meso} = V_{total} - V_{micro}$; the value in parentheses gives the extent of the decrease.

petroleum refining.[58] Steaming of zeolite Y results in not only dealumination but also generates mesopores. Commercial steamed zeolite Y (CBV720, Zeolyst International) was used as a support for the Ru complexes, which contain both micro- and meso-pores. The pore size distribution was calculated from the N_2 adsorption isotherm (Table 1 and Fig. S2, ESI†).

Table 1 shows that immobilization of both CAAC Ru complexes on the HY zeolite results in a similar decrease in the specific surface area, and both micro- and mesoporous volume, by an average of 20%. Volkov *et al.*[59] identified 10–20 nm mesopores in steamed zeolite Y (CVB 720). The size of the CAAC Ru complexes **1** (1.5 × 1.1 × 0.7 nm) and **2** (1.6 × 1.2 × 0.7 nm) is larger than the pore opening of the micropores of zeolite Y, so deposition of the complexes is expected to be in the mesopores and on the outer surface of the zeolite crystals.

Chemical analysis reveals that the aluminum content of HY is 1.05 mmol g_{cat}^{-1}, although a large proportion of the aluminum is in extra-framework positions. The concentration of framework aluminum, *i.e.*, the ion-exchange capacity, was determined *via* temperature-programmed ammonia evolution (TPAE) measurements of the ammonium form of zeolite Y (Fig. S3, ESI†). The FT-IR spectra obtained from the adsorption of pyridine gave information about the Brønsted acid–Lewis acid character of the zeolite (Fig. S4 and Table S1, ESI†).

Results confirm that the amount of exchangeable protons in H-Y is about 0.29–0.30 mmol g_{cat}^{-1} (Fig. S3 and Table S1, ESI†), although the majority of them (about 90%) are not accessible for large Ru complexes. The quaternary ammonium ions of the CAAC complexes can exchange zeolitic protons located on the outer surface of the crystals as well as those inside the crystals that are accessible through the mesopores.

Following the impregnation of complexes **1** and **2** in zeolite Y to provide supported catalysts **3** and **4** (a detailed description of the applied wet impregnation method can be found in the ESI†), inductively coupled plasma optical emission spectrometry (ICP-OES) analysis revealed a Ru content of 0.010 mmol g_{cat}^{-1} and 0.009 mmol g_{cat}^{-1} for catalysts **3** and **4**, respectively. This is approximately equal to a 0.1 wt% ruthenium content. On the other hand, no sulfur – triflate residue – was detected, indicating that the catalyst impregnation was taking place presumably not through simple physical adsorption but instead *via* ion exchange. Under normal reaction conditions (Table 2) neither complex **1** nor **2** was leached from the supported catalyst in the aqueous reaction medium.

An electrospray ionization time-of-flight mass spectrometry (ESI-TOF MS; Fig. S6 and S7, ESI†) and matrix assisted laser desorption ionization-time of flight mass spectrometry (MALDI-TOF MS; Fig. S9, ESI†) study of catalyst of **3** revealed the presence of the intact complex (**1**) at *m/z* 669 ($C_{34}H_{45}ON_2Cl_2Ru^+$). By contrast, in the case of catalyst **4**, the intact complex (**2**) could not be detected using either ESI-TOF MS or MALDI-TOF MS, presumably due to the very strong bidentate binding of **2** on the surface of the zeolite. However, characteristic fragment ions of the ligand of **2** at *m/z* 335 ($C_{23}H_{31}N_2^+$) and 347 ($C_{24}H_{31}N_2^+$) could be observed in the ESI-TOF (Fig. S8, ESI†) and LDI-TOF (Fig. S10, ESI†) spectra. (Details of the MS investigations are summarized in the ESI.†)

Fig. 2 reveals that the Ru complex (**2**) is bound to the zeolite support since the characteristic X-ray emission peaks (K_α and K_β) of Ru are present in the X-ray fluorescence (XRF) spectrum at energies of 19.3 keV and 21.7 keV, respectively, as indicated by the vertical dashed green lines. Nevertheless, these peaks are absent from the XRF spectrum of the unloaded zeolite.

Table 2 Ammonia borane (**AB**) dehydrogenation experiments at 0.3 M **AB** concentration using homogeneous catalysts (**1** and **2**) and zeolite-supported catalysts (**3** and **4**)

Entry	Cat.	Cat. load[e] [mol%]	[ppm]	Time [h]	Equiv. of hydrogen generated	Initial TOF [$mol_{H_2}\ mol_{cat}^{-1}\ h^{-1}$]	TON [$mol_{H_2}\ mol_{cat}^{-1}$]
1[a]	**1**	0.050	500	1	2.06	116	4120
2[a]	**3**	0.050	500	4	2.76 (±0.05)	43	5430 ± 92[d]
3[a]	**2**	0.050	500	1	1.95	124	3900
4[a]	**4**	0.050	500	4	2.81 (±0.01)	43	5530 ± 18[d]
5[a]	**3**	0.010	100	12	2.16 (±0.15)	105	21 300 ± 1256[d]
6[a]	**4**	0.010	100	12	2.61 (±0.01)	101	25 700 ± 90[d]
7[b]	**1**	0.005	50	20	2.11	115	41 200
8[b]	**3**	0.005	50	24	1.52 (±0.03)	142	30 100 ± 532[d]
9[b]	**2**	0.005	50	20	2.18	125	43 600
10[b]	**4**	0.005	50	24	2.51 (±0.01)	142	49 375 ± 178[d]
11	**3**	0.002	20	36	1.01 (±0.03)	111	45 000 ± 1350[d]
12	**4**	0.002	20	36	1.41 (±0.01)	138	62 200 ± 450[d]
13[c]	**1**	0.001	10	36	0.58	137	56 000
14[b]	**3**	0.001	10	36	0.80 (±0.1)	150	78 200 ± 8825[d]
15[c]	**2**	0.001	10	36	0.88 (±0.05)[d]	144	86 100 ± 3971[d]
16[b]	**4**	0.001	10	36	0.81 (±0.1)	153	79 000 ± 7860[d]

[a] Conditions: [**AB**] = 0.30 M, T = 25 °C, H_2O solvent, volume = 2 mL. [b] Volume = 5 mL. [c] Volume = 8 mL. [d] Average of three runs. [e] Relative to **AB**.

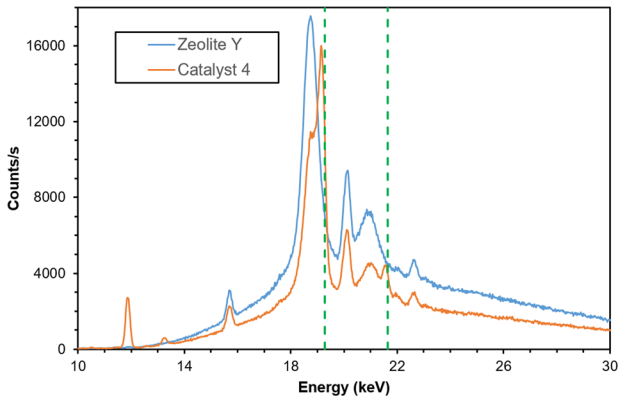

Fig. 2 Overlaid X-ray fluorescence (XRF) spectra of the zeolite support (blue) and impregnated catalyst **4** (orange).

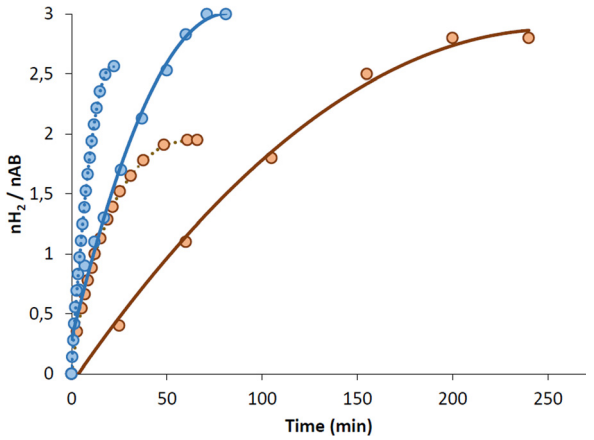

Fig. 3 Comparison of the H_2-release kinetics using homogeneous catalyst **2** (dashed line) and zeolite-supported catalyst **2** (catalyst **4**, solid line). Blue, 2000 ppm catalyst loading; brown, 500 ppm catalyst loading. Conditions: [**AB**] = 0.30 M, T = 25 °C, H_2O solvent.

The parent HY zeolite and catalyst **3** and **4** were also investigated using diffuse reflectance infrared Fourier transform (DRIFT) spectroscopy. It was found that, due to the presumably low content of complex **1** and **2** in catalyst **3** and **4**, respectively, the IR bands of the CAAC complexes could not be detected. These studies revealed, however, that the freshly prepared catalysts **3** and **4** (using methanol as solvent) contained a significant amount of adsorbed methanol, giving high-intensity IR bands (Fig. S5, ESI† spectra b and c). This observation is in line with literature reports that most of the zeolite protons may interact with methanol at room temperature, forming methoxy species.[60,61] This may explain the significantly lower **1** and **2** catalyst adsorption capacity compared with the Skowerski complex, which is impregnated using dichloromethane solvent (Fig. 1).[57] Interestingly, it was also found that during the catalytic **AB** hydrolytic dehydrogenation reactions the methoxy species associated with Brønsted acid sites are replaced by NH_4^+ cations (Fig. S5, ESI† spectra d and e).

AB hydrolytic dehydrogenation. Investigation of the ammonia borane dehydrogenation activity using zeolite-Y-supported catalysts **3** and **4** was carried out at room temperature in aqueous solution exposed to the air (Scheme 2). The solid catalyst **3** or **4** was added in one portion to the solution of **AB** (0.0960 or 0.30 M), upon which gas evolution was immediately observed, which was collected using a gas burette. Qualitative analysis of the released gas using GC equipped with a TCD detector confirmed that the formed gas was exclusively H_2. An ^{11}B NMR investigation of the reaction mixture revealed that the reaction product contained only borate species besides the starting material (Fig. S1, ESI†).[31]

In a blank test, using mesoporous zeolite Y without any impregnated complex did not initiate hydrogen release. Removal of the solid Ru catalyst *via* filtration in the course of the reaction resulted in the immediate cessation of hydrogen release.

Based on the kinetic plots of the reaction carried out at different **AB** concentrations there was no significant difference in the starting reaction rates observed, which is in line with the literature data indicating that the hydrolytic dehydrogenation of **AB** is zero order with respect to [**AB**].[62] Comparing the catalytic activity of homogeneous catalyst **2** with the zeolite-Y-supported catalyst **4** (carrying complex **2**) it was found that complex **2** initiated a significantly faster reaction at 2000 and 500 ppm loadings, whereas zeolite-supported catalyst **4** resulted in a higher released-H_2/**AB** ratio, actually a higher **AB** conversion. The slower reaction using catalyst **4** can be explained *via* some diffusion inhibition, which can be expected under heterogeneous reaction conditions.[63] An increase in the dehydrogenation rate due to the adsorption of ammonia borane adjacent to the anchored complex may also occur. The higher H_2/**AB** ratio (*i.e.*, yield) and longer lifetime, however, indicate that the zeolite

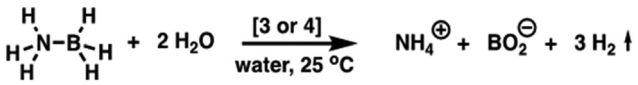

Scheme 2 Hydrolytic dehydrogenation of ammonia borane (**AB**) under air in neat water using catalysts **3** and **4**.

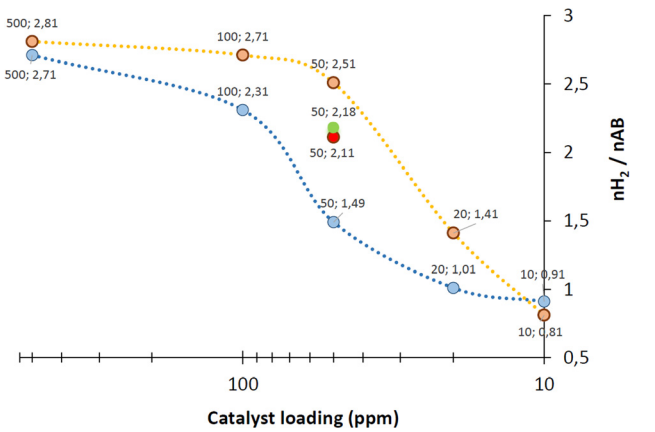

Fig. 4 H_2/**AB** yield *versus* catalyst loading (red, catalyst **1**; green, catalyst **2**; blue, catalyst **3**; orange, catalyst **4**). Conditions: [**AB**] = 0.096 M, T = 25 °C, H_2O solvent.

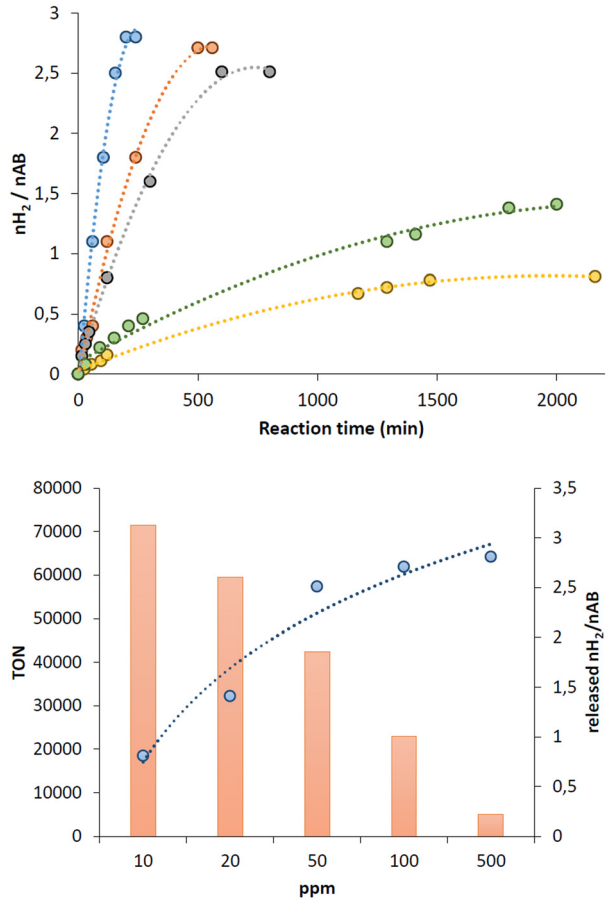

Fig. 5 (Top) Kinetic profile of H_2 release at different loadings of catalyst **4**. Blue, 0.05 mol% (500 ppm); orange, 0.01% (100 ppm); grey, 0.005 mol% (50 ppm); green, 0.002 mol% (20 ppm); yellow, 0.001 mol% (10 ppm). (Bottom) Released H_2 equivalent *versus* the TON at different loadings of catalyst **4** (where the corresponding reaction time and conditions for each run are given in Table 2, entries 4, 6, 10, 12 and 16). Conditions: [**AB**] = 0.0960 M, T = 25 °C, H_2O solvent.

support may stabilize the cyclic alkyl amino carbene Ru complexes, thus preventing their degradation (Table 2 and Fig. 3).[64–66]

Comparing the catalytic activity of **3** and **4** it can be clearly seen that catalyst **4** has a significantly higher activity at 100, 50 and 20 ppm loading than catalyst **3** (Fig. 4 and Table 2.).

However, at 10 ppm there is no significant difference, indicating that at this loading the activity significantly drops for both catalysts (Fig. 4). It is also worth mentioning that at the 50 ppm level using homogeneous catalysts **1** and **2** the H_2/**AB** values are 2.11 and 2.18, respectively.

These values are higher than that of catalyst **3** (1.52 ± 0.03) but lower than that of catalyst **4** (2.51 ± 0.01) indicating that catalyst **4** is the most active among all the examined catalysts (**1**–**4**) at a 50 ppm loading (Fig. 4). However, at the 10 ppm level all the catalysts showed similarly low H_2/**AB** values (0.58–0.81), although the TON was found to be as high as 79 000 mol_{H_2} mol_{cat}^{-1}, which are comparable to the data observed at homogeneous condition.

Although lowering the catalyst loading led to a slight drop in the H_2/**AB** ratio below the applied catalyst concentration of 500 ppm (Fig. 5), it was found that the impregnation of complex **1** and **2** in zeolite Y had a positive effect on the catalyst stability and thus on the catalyst performance. For example, at a 500 ppm loading, the H_2/**AB** ratio remains high for **3** and **4** (2.76 and 2.81), while at this loading their homogenous analogues showed a significant decrease in activity (2.06 and 1.95) (Table 2). The TOF values are lower for catalysts **3** and **4** at a high loading compared with their homogenous analogues **1** and **2**; however, as the loading was decreased below 500 ppm, the difference between the TOFs for the homogeneous and heterogeneous systems became smaller (Table 2). The lower TOF values at high loadings (above 500 ppm) might be explained by some steric effect caused by the zeolite support. Nevertheless, at a lower loading the site-specific reaction rate (*i.e.*, the TOF) becomes lower, indicating that the zeolitic steric effect becomes less dominating.

Comparing the performance of the reported heterogeneous ruthenium catalyst systems **3** and **4** with their homogeneous analogs **1** and **2** (Table 3), it can be concluded that the immobilized catalysts perform significantly better. Tentatively, the catalyst performance can be deduced from TON divided by the reaction time multiplied by catalyst and substrate concentration to obtain the so-called catalyst performance indicator (CPI). This number was applied to quantify the activity of each catalyst. Thus, the CPI values indicate that the zeolite-Y-supported

Table 3 Comparison of heterogeneous and heterogenized homogeneous ruthenium **AB** hydrolytic dehydrogenation catalyst performance (25 °C, neat water)

Entry[Ref.]	Cat.	[Ru] (mM)	[**AB**] (mM)	TOF [mol_{H_2} mol_{cat}^{-1} min^{-1}]	TON [mol_{H_2} mol_{cat}^{-1}]	Time [h]	CPI[a] (1/(h mM^2))
1[bc,67]	Ru/HAp	0.78	30	137	87 000	202	18
2[b,68]	Ru(0)/X-NW	0.05	30	135	134 100	166	539
3[b,38]	Ru(0)/CeO_2	0.19	50	361	135 100	250	56
4[b,69]	RuNi/TiO_2	0.06	100	241	71 500	73	163
5[b,70]	Ru(0)/HfO_2	0.067	100	170	175 600	500	52
6[cd]	**3**	0.0048	96	110[e]	27 950	24	2527
7[cd]	**4**	0.0048	96	125[e]	45 500	24	4114
8[d]	**3**	0.0019	96	113[e]	45 000	36	6853
9[d]	**4**	0.0019	96	153[e]	62 200	36	9472
10[cd]	**3**	0.00096	96	155[e]	78 700	36	23 720
11[cd]	**4**	0.00096	96	153[e]	79 000	36	23 810

[a] CPI: catalyst performance indicator = (TON/(reaction time (h)) × [Ru] (mM) × $[\mathbf{AB}]_0$ (mM)). [b] TON calculation is carried out with **AB** reloaded until hydrogen is released. [c] TON calculation is carried out with **AB** added only at the beginning of the reaction. [d] This work. [e] Initial TOF.

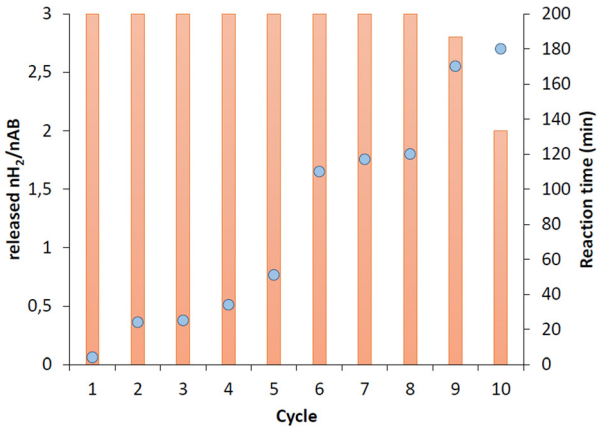

Fig. 6 Catalyst recycling. Orange columns, H_2/**AB** ratio; blue dots, reaction time in minutes (catalyst **4** loading, 5000 ppm (0.5 mol%); [**AB**] = 0.3 M; 25 °C; overall reaction time, 3 days; upon reaction completion the mixture was centrifuged, then the supernatant was decanted, and in the upcoming cycle additional **AB** solution was added to the catalyst **4**).

catalysts are among the best performing **AB**-decomposing catalyst systems so far (Table 3).

Recycling. The reusability of catalyst **4** was investigated at a 5000 ppm (0.5 mol%) loading. It was found that the catalyst can be recycled up to ten times (Fig. 6). However, it should be noted that some catalyst deactivation was observed, which is manifested in the extended reaction time for complete **AB** conversion. The 9th and 10th cycles required not only an extended reaction time but also rendered a slightly lower H_2 yield. After the 10th cycle the overall TON reached 5530 mol_{H_2} mol_{cat}^{-1}.

It is worth mentioning, that all cycles were carried out in neat water exposed to the air. The overall experiment time was three days. Even after three days, the catalyst still showed a reasonable activity. The half-life of the zeolite-supported catalyst in aqueous solution in the absence of **AB** showed that catalysts **3** and **4** are both highly stable and can be stored in water for a couple of days without any significant loss of activity.

Conclusions

The hydrolytic dehydrogenation of **AB** in neat water using zeolite-supported cyclic alkyl amino mono- and bis-carbene complexes (catalysts **3** and **4**) containing as low as 0.1 wt% ruthenium has been investigated. Comparing catalysts **3** and **4** it was found that catalyst **4** showed a higher activity than catalyst **3**. This trend is similar to the activities of catalysts **1** and **2**, indicating that the coordination of more CAAC ligands to Ru presumably improves the stability significantly and therefore the catalyst performance. None of the catalysts showed leaching in the aqueous reaction medium. The zeolite catalyst **4** showed a high activity even at concentration level as low as 50 ppm, which was found to be optimal ($n$$H_2$/$n$**AB** = 2.51) compared with its homogeneous analogues ($n$$H_2$/$n$**AB** = 2.18). Although the homogeneous catalyst systems using complexes **1** and **2** showed higher TOF values at loadings of 500 and 2000 ppm compared with their heterogeneous analogues **3** and **4**, the overall **AB** conversion was significantly higher for the zeolite-supported systems. The reported zeolite-Y-supported catalysts **3** and **4** are among the most active **AB** hydrolytic dehydrogenation ruthenium catalysts so far. Taking advantage of such heterogenization, catalyst **4** could be recycled up to 10 times at a catalyst loading of 0.5 mol% without any significant drop in the $n$$H_2$/$n$**AB** ratio.

The highest TON, 79 000 mol_{H_2} mol_{cat}^{-1}, obtained using catalyst **4** corresponds to the generation of 1.68 kg H_2 per gram of ruthenium metal. Considering that the energy content of 1.68 kg H_2 is equal to that of 6.35 L gasoline[71] and that the efficiency of hydrogen fuel cells (at ~60%) is higher than those of internal combustion engines (~20%), it could be concluded that the 1.68 kg H_2 generated using a catalyst containing 1 g of Ru metal is sufficient for a common hydrogen-fueled personal car to travel about 300 km.

Conflicts of interest

There are no conflicts to declare.

Acknowledgements

Thanks are due for the support provided by the European Union and the State of Hungary, co-financed by the European Regional Development Fund in the framework of the project no. VEKOP-2.3.2-16-2017-00013. This work was funded by grants provided by the National Competitiveness and Excellence Program, Hungary (NVKP-16-1-2016-0007). Project no. TKP2021-NKTA-34 has been also implemented with the support provided by the National Research, Development and Innovation Fund of Hungary, financed under the TKP2021-NKTA funding scheme. We thank Máté Csontos for XRF and Zoltán May for ICP-OES measurements. The authors acknowledge the financial support of the project by the Economic Development and Innovation Operative Program of Hungary, GINOP-2.3.2-15-2016-00053: Development of liquid fuels having high hydrogen content in the molecule (contribution to sustainable mobility). The Project is supported by the European Union. R. Tuba thanks the Hungarian National Research, Development and Innovation Office – NKFIH under the Grant TKP-108-9/PALY-2021. R. Tuba is grateful for the Fulbright Scholarship (2022–2023).

References

1 O. Ellabban, H. Abu-Rub and F. Blaabjerg, *Renewable Sustainable Energy Rev.*, 2014, **39**, 748–764.
2 M. Raunbak, T. Zeyer, K. Zhu and M. Greiner, *Energies*, 2017, **10**, 1934.
3 J. Chi and H. Yu, *Chin. J. Catal.*, 2018, **39**, 390–394.
4 U. Eberle, B. Müller and R. von Helmolt, *Energy Environ. Sci.*, 2012, **5**, 8780.
5 Y.-H. P. Zhang, B. R. Evans, J. R. Mielenz, R. C. Hopkins and M. W. W. Adams, *PLoS One*, 2007, **2**, e456.

6 X. Ye, Y. Wang, R. C. Hopkins, M. W. W. Adams, B. R. Evans, J. R. Mielenz and Y.-H. P. Zhang, *ChemSusChem*, 2009, **2**, 149–152.
7 Y.-H. P. Zhang, *Energy Environ. Sci.*, 2009, **2**, 272.
8 A. G. Olabi, *Energy*, 2017, **136**, 1–6.
9 S. D. Rassat, C. L. Aardahl, T. Autrey and R. S. Smith, *Energy Fuels*, 2010, **24**, 2596–2606.
10 Y. Lin and W. L. Mao, *Chin. Sci. Bull.*, 2014, **59**, 5235–5240.
11 F. H. Stephens, V. Pons and R. Tom Baker, *J. Chem. Soc., Dalton Trans.*, 2007, **2**, 2613–2626.
12 U. B. Demirci, *Int. J. Hydrogen Energy*, 2017, **42**, 9978–10013.
13 A. Staubitz, A. P. M. Robertson and I. Manners, *Chem. Rev.*, 2010, **110**, 4079–4124.
14 A. S. Brioche, Boron, **https://pubs.usgs.gov/periodicals/mcs2020/mcs2020-boron.pdf**.
15 P. Argust, *Biol. Trace Elem. Res.*, 1998, **66**, 131–143.
16 G. Moussa, R. Moury, U. B. Demirci and P. Miele, *Int. J. Hydrogen Energy*, 2013, **38**, 7888–7895.
17 C. H. Liu, Y. C. Wu, C. C. Chou, B. H. Chen, C. L. Hsueh, J. R. Ku and F. Tsau, *Int. J. Hydrogen Energy*, 2012, **37**, 2950–2959.
18 M. Chandra and Q. Xu, *J. Power Sources*, 2007, **168**, 135–142.
19 M. Chandra and Q. Xu, *J. Power Sources*, 2006, **156**, 190–194.
20 Q. Xu and M. Chandra, *J. Power Sources*, 2006, **163**, 364–370.
21 Z. P. Li, B. H. Liu, J. K. Zhu, N. Morigasaki and S. Suda, *J. Alloys Compd.*, 2007, **437**, 311–316.
22 V. Sit, R. A. Geanangel and W. W. Wendlandt, *Thermochim. Acta*, 1987, **113**, 379–382.
23 H. L. Jiang and Q. Xu, *Catal. Today*, 2011, **170**, 56–63.
24 C. Yüksel Alpaydın, S. K. Gülbay and C. Ozgur Colpan, *Int. J. Hydrogen Energy*, 2020, **45**, 3414–3434.
25 P. V. Ramachandran and P. D. Gagare, *Inorg. Chem.*, 2007, **46**, 7810–7817.
26 S. Akbayrak and S. Özkar, *Int. J. Hydrogen Energy*, 2018, **43**, 18592–18606.
27 J. A. Buss, G. A. Edouard, C. Cheng, J. Shi and T. Agapie, *J. Am. Chem. Soc.*, 2014, **136**, 11272–11275.
28 M. Hasenbeck, J. Becker and U. Gellrich, *Angew. Chem., Int. Ed.*, 2020, **59**, 1590–1594.
29 A. J. M. Miller and J. E. Bercaw, *Chem. Commun.*, 2010, **46**, 1709–1711.
30 A. Rossin and M. Peruzzini, *Chem. Rev.*, 2016, **116**, 8848–8872.
31 M. Nagyházi, G. Turczel, P. T. Anastas and R. Tuba, *ACS Sustainable Chem. Eng.*, 2020, **8**, 16097–16103.
32 D. H. A. Boom, A. R. Jupp and J. C. Slootweg, *Chem.– Eur. J.*, 2019, **25**, 9133–9152.
33 Y. Luo, L. Sun, F. Xu and Z. Liu, *J. Mater. Chem. A*, 2018, **6**, 7293–7309.
34 E. M. Titova, E. S. Osipova, A. A. Pavlov, O. A. Filippov, S. V. Safronov, E. S. Shubina and N. V. Belkova, *ACS Catal.*, 2017, **7**, 2325–2333.
35 W. Chen, J. Ji, X. Feng, X. Duan, G. Qian, P. Li, X. Zhou, D. Chen and W. Yuan, *J. Am. Chem. Soc.*, 2014, **136**, 16736–16739.
36 W. Chen, J. Ji, X. Duan, G. Qian, P. Li, X. Zhou, D. Chen and W. Yuan, *Chem. Commun.*, 2014, **50**, 2142–2144.
37 A. Aijaz, A. Karkamkar, Y. J. Choi, N. Tsumori, E. Rönnebro, T. Autrey, H. Shioyama and Q. Xu, *J. Am. Chem. Soc.*, 2012, **134**, 13926–13929.
38 S. Akbayrak, Y. Tonbul and S. Özkar, *Dalton Trans.*, 2016, **45**, 10969–10978.
39 X. Hu, M. Soleilhavoup, M. Melaimi, J. Chu and G. Bertrand, *Angew. Chem., Int. Ed.*, 2015, **54**, 6008–6011.
40 X. Zhang, L. Kam, R. Trerise and T. J. Williams, *Acc. Chem. Res.*, 2017, **50**, 86–95.
41 A. L. Colebatch and A. S. Weller, *Chem. – Eur. J.*, 2019, **25**, 1379–1390.
42 A. D. Sutton, A. K. Burrell, D. A. Dixon, E. B. Garner, J. C. Gordon, T. Nakagawa, K. C. Ott, J. P. Robinson and M. Vasiliu, *Science*, 2011, **331**, 1426–1429.
43 M. Soleilhavoup and G. Bertrand, *Acc. Chem. Res.*, 2015, **48**, 256–266.
44 M. N. Hopkinson, C. Richter, M. Schedler and F. Glorius, *Nature*, 2014, **510**, 485–496.
45 M. Koy, H. J. Altmann, B. Autenrieth, W. Frey and M. R. Buchmeiser, *Beilstein J. Org. Chem.*, 2015, **11**, 1632–1638.
46 M. Nagyházi, G. Turczel, Á. Balla, G. Szálas, I. Tóth, G. T. Gál, B. Petra, P. T. Anastas and R. Tuba, *ChemCatChem*, 2020, **12**, 1953–1957.
47 K. Skowerski, G. Szczepaniak, C. Wierzbicka, Ł. Gułajski, M. Bieniek and K. Grela, *Catal. Sci. Technol.*, 2012, **2**, 2424–2427.
48 R. Zhong, A. C. Lindhorst, F. J. Groche and F. E. Kühn, *Chem. Rev.*, 2017, **117**, 1970–2058.
49 R. Kore, M. Tumma and R. Srivastava, *Catal. Today*, 2012, **198**, 189–196.
50 A. Corma, E. Gutiérrez-Puebla, M. Iglesias, A. Monge, S. Pérez-Ferreras and F. Sánchez, *Adv. Synth. Catal.*, 2006, **348**, 1899–1907.
51 D. P. Allen, M. M. V. Wingerden and R. H. Grubbs, *Org. Lett.*, 2009, **11**, 1261–1264.
52 K.-Y. Yoon, J. Noh, Q. Gan, J. Edwards, R. Tuba, T.-L. Choi and R. Grubbs, *ChemRxiv*, DOI: **10.26434/chemrxiv-2021-270bw**.
53 H. Balcar, N. Žilková, M. Kubů, M. Mazur, Z. Bastl and J. Čejka, *Beilstein J. Org. Chem.*, 2015, **11**, 2087–2096.
54 K. Kaczanowska, M. Chwalba, J. Pastva, M. Kubů, A. Ruszczyńska, E. Bulska, H. Balcar and K. Skowerski, *Organometallics*, 2018, **37**, 1837–1844.
55 A. Jana and K. Grela, *Chem. Commun.*, 2017, **54**, 122–139.
56 A. Dewaele, F. Verpoort and B. Sels, *ChemCatChem*, 2016, **8**, 3010–3030.
57 J. Pastva, K. Skowerski, S. J. Czarnocki, N. Žilková, J. Čejka, Z. Bastl and H. Balcar, *ACS Catal.*, 2014, **4**, 3227–3236.
58 E. T. C. Vogt and B. M. Weckhuysen, *Chem. Soc. Rev.*, 2015, **44**, 7342–7370.
59 R. L. Volkov, V. N. Kukin, P. A. Kots, I. I. Ivanova and N. I. Borgardt, *ChemPhysChem*, 2020, **21**, 275–279.
60 X. Z. Jiang, *J. Mol. Catal. A: Chem.*, 1997, **121**, 63–68.
61 L. Kubelková, J. Nováková and K. Nedomová, *J. Catal.*, 1990, **124**, 441–450.

62 Q. Yao, Z. H. Lu, K. Yang, X. Chen and M. Zhu, *Sci. Rep.*, 2015, **5**, 1–11.
63 C. Sievers, S. L. Scott, Y. Noda, L. Qi, E. M. Albuquerque and R. M. Rioux, *ACS Catal.*, 2016, **6**(12), 8286–8307.
64 Á. Zsigmond, K. Bogár and F. Notheisz, *J. Catal.*, 2003, **213**, 103–108.
65 W. Luo, W. Cao, P. C. A. Bruijnincx, L. Lin, A. Wang and T. Zhang, *Green Chem.*, 2019, **21**, 3744–3768.
66 Z. Li, D. Wang, Y. Wu and Y. Li, *Natl. Sci. Rev.*, 2018, **5**, 673–689.
67 S. Akbayrak, P. Erdek and S. Özkar, *Appl. Catal., B*, 2013, **142–143**, 187–195.
68 S. Akbayrak and S. Özkar, *Dalton Trans.*, 2014, **43**, 1797–1805.
69 S. Akbayrak, S. Tanyildizi, I. Morkan and S. Özkar, *Int. J. Hydrogen Energy*, 2014, **39**, 9628–9637.
70 E. B. Kalkan, S. Akbayrak and S. Özkar, *Mol. Catal.*, 2017, **430**, 29–35.
71 Alternative Fuels Data Center, **https://afdc.energy.gov/fuels/properties**.